



Fermi National Accelerator Laboratory

FERMILAB-Conf-91/216

**Measurement of  $\bar{p}p$  Elastic Scattering  
Parameters at  $\sqrt{s}=1.8$  TeV**

S. Shukla

*Fermi National Accelerator Laboratory  
P.O. Box 500, Batavia, Illinois 60510*

August 1991

\* Presented at the *International Conference on Elastic and Diffractive Scattering*, La Biodola, Italy,  
May 22-25, 1991.





# Measurement of $\bar{p}p$ Elastic Scattering Parameters at $\sqrt{s}=1.8$ TeV

Shekhar Shukla

Fermi National Accelerator Laboratory, U.S.A.

for the E710 Collaboration.

N.A. Amos<sup>a</sup>, C. Avila<sup>a</sup>, W.F. Baker<sup>a</sup>, M. Bertani<sup>b</sup>, M.M. Block<sup>c</sup>, D.A. Dimitroyannis<sup>d</sup>, D.P. Eartly<sup>a</sup>, R.W. Ellsworth<sup>e</sup>, G. Giacomelli<sup>b</sup>, B. Gomez<sup>a</sup>, J.A. Goodman<sup>d</sup>, C.M. Guss<sup>c</sup>, A.J. Lennox<sup>a</sup>, M.R. Mondardini<sup>b</sup>, J.P. Negret<sup>a</sup>, J. Orear<sup>f</sup>, S.M. Pruss<sup>a</sup>, R. Rubinstein<sup>a</sup>, S. Sadr<sup>c</sup>, J.C. Sanabria<sup>a</sup>, S. Shukla<sup>a</sup>, M. Spagnoli<sup>b</sup>, I. Veronesi<sup>b</sup> and S. Zucchelli<sup>b</sup>.

<sup>a</sup> Fermi National Accelerator Laboratory

<sup>b</sup> Università di Bologna and Istituto Nazionale di Fisica Nucleare

<sup>c</sup> Northwestern University

<sup>d</sup> University of Maryland

<sup>e</sup> George Mason University

<sup>f</sup> Cornell University

A measurement of the total nuclear cross section,  $\sigma_t$ , the ratio of the real to the imaginary part of the forward nuclear elastic scattering amplitude,  $\rho$ , and the nuclear slope parameter,  $B$ , for  $\bar{p}p$  elastic scattering at  $\sqrt{s} = 1.8$  TeV, is presented. We find  $\sigma_t = 72.8 \pm 3.1$  mb,  $\rho = 0.140 \pm 0.069$  and  $B = 16.99 \pm 4.7$  (GeV/c)<sup>-2</sup>.

## 1. Introduction

The elastic differential cross section for  $\bar{p}p$  scattering is given by a sum of three terms - a Coulomb term, a nuclear term and an interference term.

$$\frac{d\sigma}{dt} = \frac{d\sigma_c}{dt} + \frac{d\sigma_{cn}}{dt} + \frac{d\sigma_n}{dt} \quad (1)$$

where  $t$  is the 4-momentum transfer squared. The three terms on the right hand side are given by,

$$\frac{d\sigma_c}{dt} = \frac{4\pi\alpha^2(\hbar c)^2 G^4(t)}{|t|^2} \quad (2)$$

$$\frac{d\sigma_n}{dt} = \frac{\sigma_t^2(1+\rho^2)}{16\pi(\hbar c)^2} e^{-B|t|} \quad (3)$$

$$\frac{d\sigma_{cn}}{dt} = \frac{\alpha(\rho - \alpha\phi)\sigma_t G^2(t)}{|t|} e^{B|t|/2} \quad (4)$$

where,

$G(t)$  is the electromagnetic form factor of the proton, written as,

$$G(t) = \left(1 + \frac{|t|}{.71}\right)^{-2}$$

$\sigma_t$  is the total nuclear cross section,  $B$  is the nuclear slope parameter,  $\rho$  is the ratio of the real to the imaginary part of the forward nuclear elastic scattering amplitude,  $\phi$  is the phase of the

Coulomb amplitude relative to the nuclear amplitude<sup>1</sup>, and  $\alpha$  is the fine structure constant. At very small values of  $|t|$ , the Coulomb term dominates. At larger values of  $|t|$ , the scattering is almost entirely nuclear. In some intermediate range around  $|t| = .001$  (GeV/c)<sup>2</sup>, there is a significant contribution from the interference term. Measurements of elastic distributions in this  $t$ -range are needed to determine  $\rho$ .

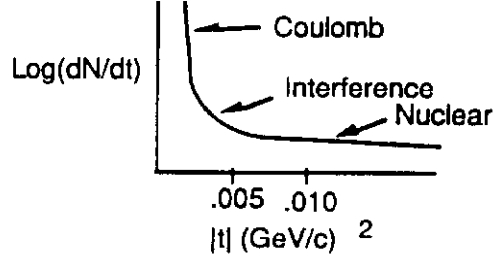


Fig 1 The Coulomb, nuclear and interference region.

## 2. $dN/dt$ in terms of $N_{inel}$ , $\sigma_t$ , $\rho$ and $B$

The number of particles scattered per unit  $t$ -interval is given by,

$$\frac{dN}{dt} = L \frac{d\sigma}{dt}$$

where  $L$  is the luminosity. Writing the total nuclear interaction rate,  $N_t = L\sigma_t$ , as the sum of the elastic rate  $N_n$ , and the inelastic interaction rate  $N_{inel}$ , we have,

$$N_n + N_{inel} = L\sigma_t \quad (5)$$

The total elastic rate is,

$$\begin{aligned} N_n &= \int_0^{\infty} dt |t| \frac{dN_n}{dt} \\ &= \int_0^{\infty} dt |t| L \frac{\sigma_t^2 (1 + \rho^2)}{16\pi(\hbar c)^2} e^{-B|t|} \\ &= L \frac{\sigma_t^2 (1 + \rho^2)}{16\pi(\hbar c)^2 B} \end{aligned} \quad (6)$$

Substituting eq. 6 into eq. 5, we get,

$$L = \frac{N_{inel}}{\sigma_t \left( 1 - \frac{\sigma_t (1 + \rho^2)}{16\pi B (\hbar c)^2} \right)} \quad (7)$$

Using eq. 7 for luminosity, we can write the contributions to the elastic differential cross section in terms of  $N_{inel}$ ,  $\sigma_t$ ,  $\rho$  and  $B$ , as,

$$\frac{dN_n}{dt} = \frac{N_{inel} \sigma_t (1 + \rho^2)}{16\pi(\hbar c)^2 \left( 1 - \frac{\sigma_t (1 + \rho^2)}{16\pi(\hbar c)^2 B} \right)} e^{-B|t|} \quad (8)$$

$$\frac{dN_c}{dt} = \frac{4\pi\alpha^2 (\hbar c)^2 N_{inel} G^4(t)}{|t|^2 \sigma_t \left( 1 - \frac{\sigma_t (1 + \rho^2)}{16\pi(\hbar c)^2 B} \right)} \quad (9)$$

$$\frac{dN_{cn}}{dt} = \frac{\alpha(\rho - \alpha\phi) G^2(t) N_{inel}}{|t| \left( 1 - \frac{\sigma_t (1 + \rho^2)}{16\pi(\hbar c)^2 B} \right)} e^{-B|t|/2} \quad (10)$$

## 3. Elastic Scattering Detectors

The apparatus was located around the E0 interaction region, as shown in fig 2. There were elastic scattering detectors, which we called pots, at four locations along the beam axis. At each location, there was a pot above and another below the beam.

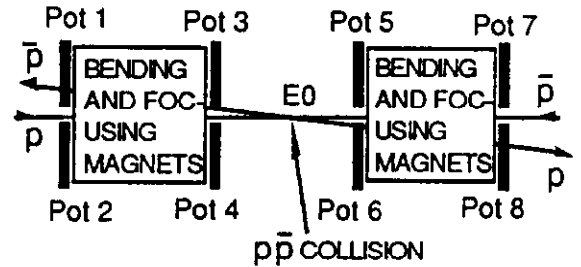


Fig 2 Location of detectors (pots).

Pots 1,2,7 and 8, which we call the outer pots, were embedded in the magnetic

lattice of the accelerator. Their vertical effective distances from E0 were  $\sim 80$  m. Pots 3, 4, 5 and 6 were in a straight section around E0, each of them  $\sim 25$  m from E0.

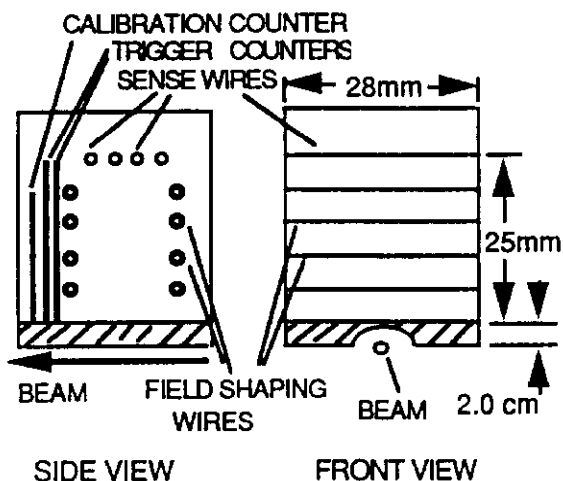


Fig 3 Elastic scattering detector.

Each pot contained a drift chamber with four sense wires (fig 3), two scintillation counters for triggering purposes and a scintillation counter, with several holes and edges, for calibration of the chamber. The vertical coordinate (y-coordinate), was measured from drift time with a resolution of  $\sim 80\mu\text{m}$ . The horizontal coordinate transverse to the beam (x-coordinate) was measured using charge division. The latter did not work very well in many of the runs. In our analysis so far, charge division has not been used to measure the scattering angle.

The assembly was housed in a thin walled metal vessel mounted on bellows (fig 4). The bellows allowed the detector to be moved close to the beam, or retracted, as needed. There was a groove running along the bottom of the pot to let the beam through.

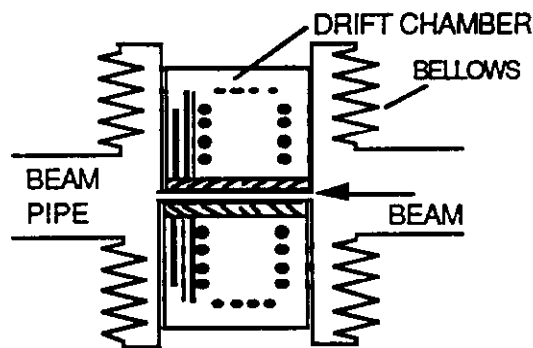


Fig 4 Pots mounted on the beam pipe.

#### 4. Data taking for elastic events.

We had two kinds of elastic triggers, the OO and the II. The OO required at least one particle in the outer pots on either side. The II trigger had a similar requirement for the inner pots. For data at very small angles, as those used in the analysis for  $\rho$ , we used the outer pots. The data was taken in dedicated runs during two periods in November 1988 and December 1988. Six bunches of protons collided with six bunches of antiprotons. The beams were scraped to enable the pots go to small angles. The scraping reduced the emittance by a factor of 4. The luminosity after scraping was  $\sim 10^{26} \text{ cm}^2 \text{ s}^{-1}$ . The active region of the chambers was 2.2 mm from the center of the beam. The t-range covered by the detectors was  $0.0006 \leq |t| \leq 0.142 (\text{GeV}/c)^2$ .

#### 5. The Scattering Angle.

The projection of the scattering angle in the horizontal plane,  $\theta_x$ , can be written in terms of the displacement  $x$  of the scattered particle from the ideal orbit, recorded at the detector, the displacements  $x_0$  and  $z_0$  in the x and z directions of the interaction from the center of the interaction region, the

initial angle  $\alpha_x$  of the colliding particle with respect to the ideal orbit, and the transport matrix elements between the center of the interaction region and the detector,  $L_x$  and  $m_x$ , as,

$$\theta_x = \frac{(x - \delta x) - m_x x_0 - \alpha_x L_x}{L_x + m_x z_0}$$

where  $\delta x$  is the difference between the actual position of the particle at the detector and the recorded position, due to the resolution of the detector.

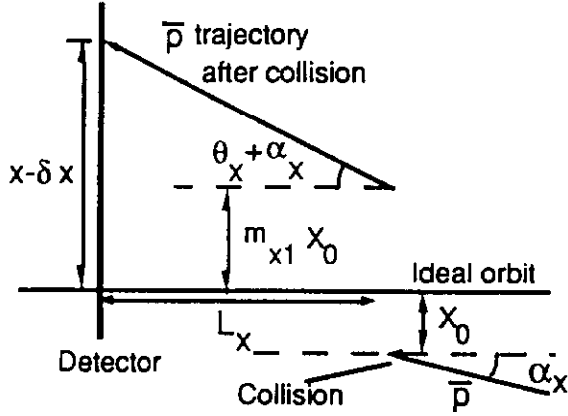


Fig 5 Trajectory of the scattered particle.

For small values of  $m_x z_0 / L_x$  and  $m_y z_0 / L_y$ , we can write,

$$\theta_x = \frac{x - X_0}{L_x}, \quad \theta_y = \frac{y - Y_0}{L_y} \quad (11)$$

where,

$$X_0 = \delta x + m_x x_0 + \alpha_x L_x$$

$$Y_0 = \delta y + m_y y_0 + \alpha_y L_y$$

## 6. Function fit to y-distributions

We define,

$$f\left(\frac{(x - X_0)^2}{L_x^2} + \frac{(y - Y_0)^2}{L_y^2}\right) = \frac{p^2}{L_x L_y} F(p^2 \theta^2)$$

where  $p$  is the momentum of the

scattered particle, and for small  $\theta$ ,

$$F(p^2 \theta^2) = F(|t|) = \frac{dN_c}{dt} + \frac{dN_{cn}}{dt} + \frac{dN_n}{dt}$$

The three terms on the right side are given by equations 8, 9 and 10. The number of events in which an elastically scattered particle strikes a strip of width  $dy$  while the other particle strikes the other detector, is given by,

$$\begin{aligned} \frac{dN}{dy} = & \int_{-\infty}^{\infty} \int_{-\infty}^{\infty} \int_{x_1}^{x_2} \int_{x_1'}^{x_2'} \int_{y_1}^{y_2} dX_0 dY_0 dx dx' dy' \\ & \times \frac{\exp(-X_0^2 / 2\sigma_{X_0}^2) \exp(-Y_0^2 / 2\sigma_{Y_0}^2)}{\sqrt{2\pi}\sigma_{X_0} \sqrt{2\pi}\sigma_{Y_0}} \\ & \times f\left[\frac{(x - X_0)^2}{L_x^2} + \frac{(y - Y_0)^2}{L_y^2}\right] \\ & \times \frac{\exp[-(x - X_0 - (x' L_x / L_x'))^2 / 2\sigma_{x'}^2]}{\sqrt{2\pi}\sigma_{x'}} \\ & \times \frac{\exp[-(y - Y_0 - (y' L_y / L_y'))^2 / 2\sigma_{y'}^2]}{\sqrt{2\pi}\sigma_{y'}} \end{aligned}$$

where  $x_1$  and  $x_2$  are the x-limits of the detector in pot 1, and  $x_1', x_2'$  and  $y_1', y_2'$  are the x and y limits of the detector in pot 8. We have taken the distributions in  $X_0$  and  $Y_0$  to be gaussians with widths  $\sigma_{X_0}$  and  $\sigma_{Y_0}$  respectively.

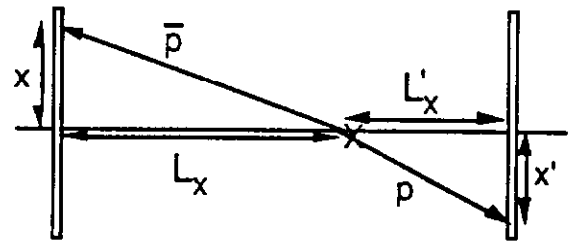


Fig 6 Scattering in the x-z plane.

The integral was written as a sum of

terms each of which factorizes into a function of  $y$  and a function of  $N_{inel}$ ,  $\sigma_t$ ,  $\rho$  and  $B$ .

$$\frac{dN}{dy} = \sum_i E_i'(N_{inel}, \sigma_t, \rho, B) K_i(y) \quad (12)$$

This function, with  $N_{inel}$  determined from our measurement of the inelastic interaction rate, was fit to the experimental distributions to extract the values of  $\sigma_t$ ,  $\rho$  and  $B$ .

### 7. Measurement of the Inelastic Rate

We had ring-shaped scintillation counters covering a pseudorapidity range from  $\sim 4.0$  to  $6.5$  on either side of the interaction region and drift chambers for tracking in the pseudo rapidity range  $6.0$  to  $6.5$  (fig 7). Our double-arm events, i.e., events in which at least one particle was recorded on either side of the collision region, were almost all due to inelastic  $\bar{p}p$  interactions. These were counted simultaneously with the recording of the elastic data.

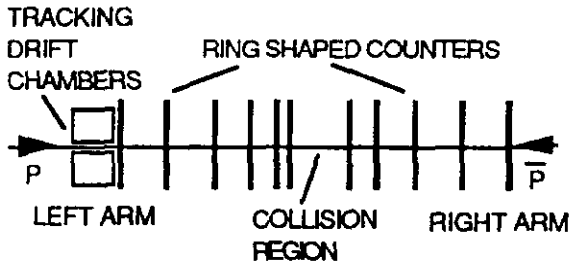


Fig 7 Counters and chambers for inelastic interaction rate.

Our single arm events, i.e., events with counters hit only on one side of the collision region, had a large background. For these we had a special run in which some proton bunches and some antiproton bunches were missing.

The rates in the counters when there were no bunch-bunch collisions in the collision region, gave the background. The ratio of single-arm  $\bar{p}p$  inelastic collisions to the double-arm events was thus measured. It was corrected for losses at small and large angles by extrapolation using the tracking chambers and counters. Then it was used to calculate the total inelastic rate in the data runs for the elastic data. For details see reference 3.

### 8. Effective Lengths and Beam widths

The  $z$ -width of the interaction region was found using the timing of particles recorded in the scintillation counters located around the interaction region. Since there were no quadrupoles between E0 and the inner pots, the distances  $L_{y3}$  and  $L_{y6}$  of the inner pots from the interaction region were known accurately. Using elastic events in which each of the two scattered particles went through an inner pot and an outer pot, we determined the effective lengths for the outer pots,  $L_{y1}$  and  $L_{y8}$ .

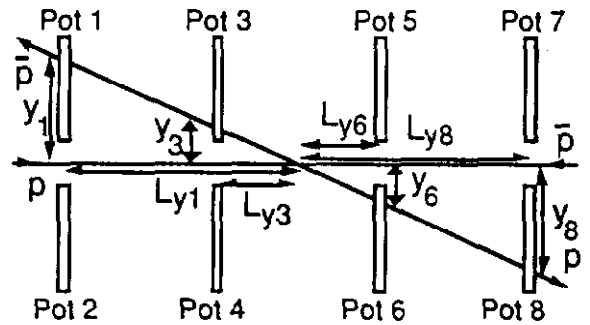


Fig 8 Determination of  $L_{eff}$ .

In addition, we obtained the vertical width  $\sigma_{yint}$  of the interaction region.

The angular divergence  $\sigma_{\theta y}$  of the beam in the vertical direction, was obtained using the width of the distribution of the difference,

$$\Delta y = y_1 - (L_{y1} / L_{y8})y_8$$

The value agreed with that obtained from the emittance of the beam.

**Table I** Beam parameters and transport matrix elements from our data (second column) and from numbers supplied by the Accelerator Group (third column).

	E710	Accelerator
$L_{x1}(\text{m})$		$45.6 \pm 5$
$L_{x8}(\text{m})$		$30.0 \pm 3$
$L_{y1}/L_{y8}$	$1.051 \pm .006$	1.073
$L_{y1}(\text{m})$	$80.4 \pm 1.0$	$80.6 \pm 1.0$
$L_{y8}(\text{m})$	$76.5 \pm 1.0$	$75.1 \pm 1.0$
$\sigma_{y\text{int}}(\text{mm})$	$0.22 \pm .04$	0.18
$\sigma_{z\text{int}}(\text{cm})$	$65 \pm 5$	
$\sigma_{\theta y}(\text{mrad})$	$3.4 \pm 12$	4.0

### 9. Selection of Elastic Events

In the off-line analysis, elastic candidates were required to have a particle in each of the two pots belonging to an elastic combination. See reference 2 for details of elastic-event selection.

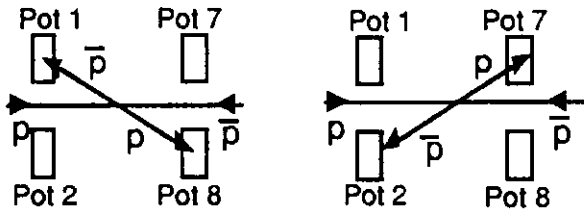


Fig 9 Events selected for elastic distributions.

Fig 10 shows the y-coordinate for the particle in pot 1 plotted against the y-

coordinate recorded in pot 8 for our elastic candidates. The elastic events lie along the positive diagonal. We see background events close to the beam. The background was approximately equal to the signal at 3 mm from the beam.

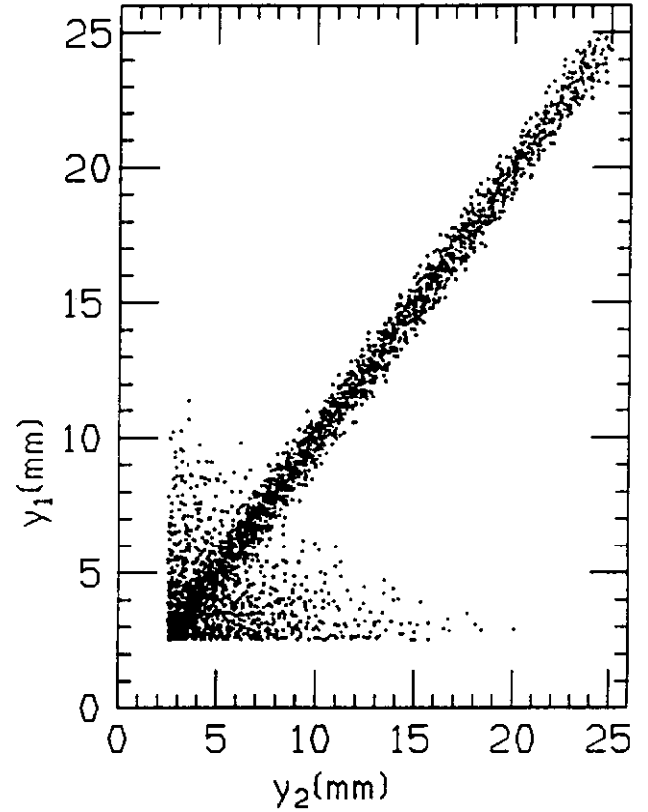


Fig 10  $y_1$  vs  $y_8$  for elastic candidates.

### 10. Background Subtraction

Due to the narrow momentum acceptance ( $<1\%$ ) of the Tevatron, we do not have a significant background, arising from inelastic  $\bar{p}p$  collisions, in our elastic sample. The background in our elastic distribution is due to uncorrelated pairs of particles in the two pots of an elastic combination. The background in the elastic sample, where the particle in pot  $i$  is at  $y=y_{ik}$  and that in pot  $j$  is at  $y=y_{jl}$ , can be written as,

$$B_{ij}(y_{ik}, y_{jl}) = cF_i(y_{ik})F_j(y_{jl}) \quad (13),$$

where  $F_i(y_{ik})$  describes the shape of the distribution of background particles in pot  $i$ , and  $c$  is a normalization constant. The distributions  $F_i(y_{ik})$  for the various pots were obtained from OO triggers in which the particles in the two arms went in the two upper pots or the two lower pots (fig 11). The normalization constant  $c$  was obtained by counting the number of events in an off-diagonal region in fig 10, and dividing by an integral of the function in eq. 13 over the same region.

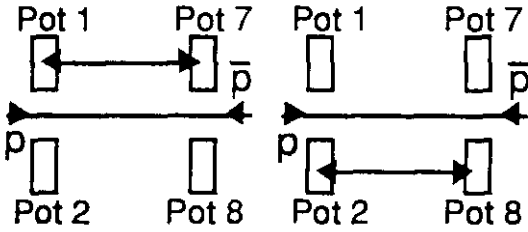


Fig 11 Events used to obtain background shapes.

### 11. Fit to the data to obtain $\rho$ , $\sigma_t$ and $B$ .

Background was subtracted from our elastic event sample as described above, and the  $y$ -distributions of the remaining events in pots 1 and 2, were obtained. These were then corrected for chamber inefficiencies. The nuclear part of the resulting distributions was fit to a gaussian to determine the forward direction in the  $y$ - $z$  plane. All  $y$ -coordinates were then measured from this forward direction and new  $y$ -distributions were obtained. These distributions were then fit to the function in eq 12 to obtain  $\sigma_t$ ,  $\rho$  and  $B$  with  $N_{inel}$  fixed.

## 12. Results.

Fig 12 shows the  $y$ -distribution of all our data with the best-fit curve superimposed. The fit gives,  $\sigma_t = 72.8 \pm 1.63$  mb,  $\rho = .140 \pm 0.048$  and  $B = 16.99 \pm .47 (\text{GeV}/c)^{-2}$ , with a  $\chi^2$  pdf of 1.29. Our results, including all uncertainties, the significant sources of which are listed in table II, are,  $\sigma_t = 72.8 \pm 3.1$  mb,  $\rho = .140 \pm 0.069$  and  $B = 16.99 \pm .47 (\text{GeV}/c)^{-2}$ .

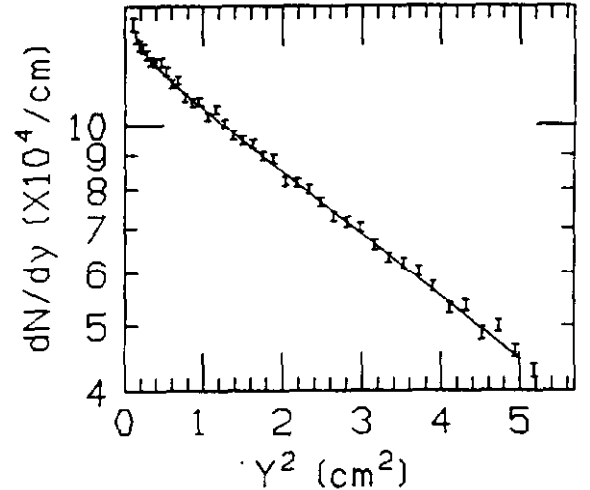


Fig 12  $y$ -distribution of elastic events.

**Table II** Main contributions to the uncertainty in  $\rho$ ,  $\sigma_t$ , and  $B$ .

Source	$\rho$	$\sigma_t$	$B$
			mb (GeV/c) <sup>-2</sup>
Fit		0.048	1.63
Background	0.043	1.27	0.093
$N_{inel}$		0.021	2.29
$L_x$		0.008	0.46
$L_y$		0.007	0.12

Fig 13 shows the  $y$ -distribution with the interference region magnified. The superimposed curves are obtained with  $\sigma_t(1+\rho^2)$  and  $B$  fixed at the best-fit values, and three different values of  $\rho$  -

0.00, 0.14 and 0.28. Fig 14 shows the variation of the  $\rho$ -value we obtain as we leave out 0.25 mm regions of the chambers near the beam.

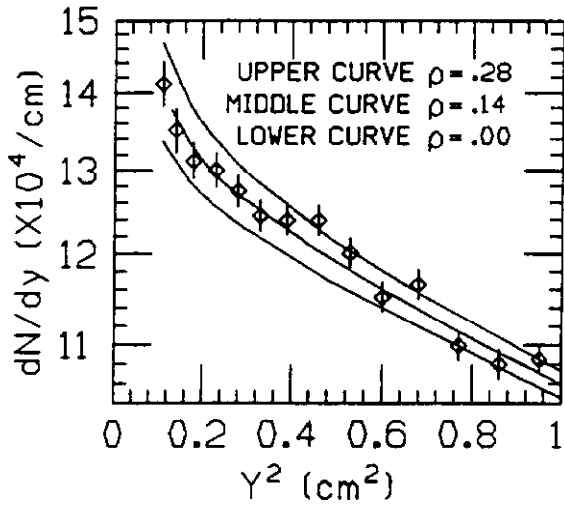


Fig 13 y-distributions of elastic events

### 13. Conclusions

The values we obtain for  $\sigma_t$  and  $\rho$  are compatible with parametrizations of  $\sigma_t$  that have the  $pp$  and  $\bar{p}p$  cross sections

becoming equal and going smoothly into a  $\log^2 s$  behavior at very high energies<sup>4,5</sup>.

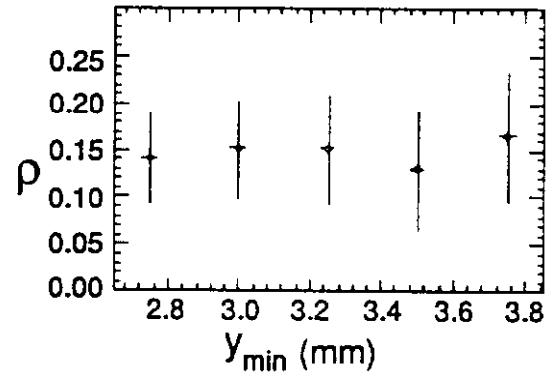


Fig 14 Stability of  $\rho$  with  $y_{\min}$ .

### 14. References

- 1) G. B. West and D. R. Yennie, Phys. Rev. 172 (1968) 1413.
- 2) N. A. Amos et al., Phys. Lett. 247B (1990) 127.
- 3) N. A. Amos et al., Phys. Lett. 243B (1990) 158.
- 4) U. Amaldi et al., Phys. Lett. 66B (1977) 390.
- 5) M. M. Block and R. N. Cahn, Phys. Lett. 149B (1984) 245.